Journal of Power Sources 217 (2012) 364–372

Contents lists available at SciVerse ScienceDirect

Journal of Power Sources

journal homepage: www.elsevier.com/locate/jpowsour

Comparison of the performances of single cell solid oxide fuel cell stacks with Ni/8YSZ and Ni/10CGO anodes with H_2S containing fuel

Sena Kavurucu Schubert [a,*], Mihails Kusnezoff [a], Alexander Michaelis [a], Sergey I. Bredikhin [b]

[a] Fraunhofer Institute for Ceramic Technologies and Systems, Winterbergstraße 28, 01277 Dresden, Germany
[b] Institute of Solid State Physics RAS, Moscow District, 2 Academician Ossipyan Str., 142432, Russia

HIGHLIGHTS

- Comparison of the effects of H_2S on SOFC stacks with Ni/8YSZ and Ni/10CGO anodes.
- H_2S poisoning progress in the SOFC anodes.
- Mechanisms of the sulfur poisoning in Ni/8YSZ and Ni/10CGO anodes.

ARTICLE INFO

Article history:
Received 14 December 2011
Received in revised form
15 May 2012
Accepted 5 June 2012
Available online 13 June 2012

Keywords:
Solid oxide fuel cells
Hydrogen sulfide
Poisoning
Degradation
Regeneration
Mechanism

ABSTRACT

The performances of single cell solid oxide fuel cell (SOFC) stacks with Ni/8YSZ (8 mol% Y_2O_3 doped ZrO_2) and Ni/10CGO (10 mol% Gd_2O_3 doped CeO_2) anodes were compared with respect to sulfur poisoning (1–50 ppm) with $H_2/H_2O/N_2$ fuel mixture at 850 °C. The mechanisms of the sulfur poisoning and regeneration of Ni/8YSZ and Ni/10CGO anodes at the triple phase boundaries are discussed. The effects of various parameters as H_2S contamination cycles, H_2S concentration, current density, H_2O concentration and contamination durations were examined. A mechanism for the progress of the sulfur poisoning in the anode is proposed. It is shown that theoretically it is possible to calculate the nickel surface area accessible for the sulfur adsorption in the anode using H_2S poisoning behavior for Ni/8YSZ anodes. The sulfur poisoning mechanisms of Ni/8YSZ and of Ni/10CGO anodes are proposed by taking into account the different oxidation mechanisms of H_2 in the anodes considered in previous studies. The higher sulfur resistance of Ni/10CGO is explained with its high mixed ionic electronic conductivity as well as its ability to adsorb H_2. Due to these properties CGO can continue electrochemical reactions even when nickel is covered with sulfur.

1. Introduction

Due to their high operating temperatures, SOFCs can be fueled with wide varieties of fuels such as hydrogen, carbon monoxide, hydrocarbons, alcohols as well as synthetic gases from natural gas, biogas and petroleum. The possibility of using such a wide range of fuels unfortunately introduces the risk of unwanted impurities, which can affect the function of the SOFC and the efficiency and durability of an SOFC system. One of the impurities is sulfur which is a well known catalyst poison and may also deactivate the anode of the solid oxide fuel cells. Sulfur and its bondings are known to exist in almost every fossil and biogenic fuel. Total sulfur concentrations in fuels can reach up to 23 ppm with 4 ppm H_2S in methane rich gases, 50 ppm in liquefied gas [1], 10 ppm in gasoline and diesel [2] and 700 ppm in biogas [3] in Germany, as an example.

It is necessary to remove sulfur compounds which are also poisons for fuel processing in SOFC systems, as well. The sulfur removal methods vary depending on the type of the fuel (liquid, gaseous or solid) and the sulfur containing component as well as the concentration to be removed. There are many types of mature (amine scrubbing, mercaptan oxidation removal process, hydrodesulfurization or desulfurization of syngas using gas–liquid absorption processes) and newer desulfurization methods where the focus is on gas-phase and liquid-phase desulfurization using solid sulfur sorbents before the reformer as well as syngas desulfurization after the reformer or gasifier in fuel cell systems [4]. Sorbent-based desulfurization processes are the most likely candidates for compact fuel processors with a potential of reducing H_2S in syngas to less than 0.1 ppmv [4]. However it is known that

* Corresponding author. Tel.: +49 351 25537819; fax: +49 351 2554211.
E-mail addresses: sena.kavurucu@ikts.fraunhofer.de, senakavurucu@yahoo.com (S. Kavurucu Schubert).

0378-7753/$ – see front matter © 2012 Elsevier B.V. All rights reserved.
http://dx.doi.org/10.1016/j.jpowsour.2012.06.020

even 0.05 ppm H_2S has an effect on the performance of SOFC, dependent on the operating conditions [5]. The desulfurization units also add complexity and extra cost to SOFC systems. Additionally a desulfurization unit breakdown may also affect the performance of the system. For this reason, it is of a great importance to understand the mechanisms behind the sulfur poisoning.

Studies on the effect of sulfur in fuel have been focused mainly on the effect of H_2S in fuel on nickel based anodes or developing alternative anode materials with high sulfur resistance. H_2S was mostly chosen as a sulfur containing component due to its stability among other sulfur containing compounds under SOFC operating conditions [6]. The studies were mainly performed with H_2/H_2O or CH_4 fuel gas mixtures and Ni/YSZ anodes. However it is difficult to generalize the effect of the poisoning on performance since degradation rates differentiate from each other due to differences in the anode material, microstructure, experimental procedures and different comparison criteria such as chemical stability, electrochemical stability, operating times, etc.

Thermodynamic calculations showed that the formation of sulfides in the anode under SOFC operating conditions is possible only with high H_2S concentrations (e.g. nickel sulfide formation with c_{H2S}>2500 ppm at 850 °C with 50% H_2 fuel) and therefore cannot explain the immediate SOFC power degradation in low ppm region. The dissociative adsorption of H_2S on nickel is commonly accepted as the mechanism behind immediate sulfur poisoning of nickel based anodes.

In some studies two stage poisoning behavior of Ni/8YSZ anodes was observed [6–8]. According to Singhal's studies [7], with addition of 2–10 ppm H_2S, the cell voltage first dropped rapidly (11.5% with 10 ppm H_2S) at 1000 °C with constant current density. A slow degradation of cell voltage (3.5%) was observed in the following 100 h. No stable phase was followed. By removing H_2S, the cell voltage regenerated. Sasaki et al. [6] tested the cells with 1–20 ppm H_2S at constant current density at 850 °C–1000 °C with 5% H_2O/95% H_2 fuel. They observed a two phase poisoning followed by a stable power at 1000 °C with 5 ppm H_2S. By removing the H_2S, the cell voltage almost reached to its initial value. However by decreasing the temperature to 850 °C, the cell voltage became unstable and was not recovered to the initial cell voltage by removing H_2S from the fuel. The voltage decreased from 0.62 V to 0.12 V under constant current of 200 $mAcm^{-2}$. During the post-mortem analysis with EDX, the authors found no sulfur but NiO traces in the anode. They explained this behavior with oxidation of Ni to NiO at lower cell voltages in which with low pH_2S the chemisorption of sulfur leads to a decrease of electrochemical sites and thus increase in anodic polarization and cell voltage drop. With relatively high pH_2S (in their case 20 ppm) further chemisorption of sulfur on nickel leads the oxidation of nickel at triple phase boundaries with oxygen ion flux from cathode and thus a further increase in anodic polarization and larger cell voltage loss. Wang et al. [8] tested the cells with 2–50 ppm H_2S with 50% H_2/1.5%H_2O/48.5%N_2 fuel. With 2 ppm H_2S the initial cell voltage drop was 12.67% in 4 min. After the following H_2S removal the cell voltage stabilized to ~99% of its initial value. A long-run test of poisoning with 50 ppm H_2S caused 16.67% voltage drop in first several minutes followed by a slow and continuous drop of 3.96% in the next 120 h. There was no stable phase after. By removing H_2S, the cell voltage recovered to ~96% after 50 h. The authors explain the irreversibility of the poisoning with the altered microstructural change of nickel surface during second phase.

Due to the high sensitivity of Ni/YSZ anodes to sulfur, some groups studied the effect of surface modification of Ni/YSZ anodes with various materials. Some of these anodes are $Sm_xCe_{1-x}O_{2-\delta}$ coated Ni/YSZ [9], Nb_2O_5 surface deposited Ni/YSZ, Mo impregnated Ni/YSZ [10] and CeO_2 coated Ni/YSZ [11]. The results showed that the surface modification of Ni/YSZ anodes may enhance the sulfur resistance of anode. Other groups substituted nickel with copper/CeO_2 and used Cu/CeO_2/YSZ as anode material [12,13]. Copper with ceria oxide is found to be more resistant to sulfur poisoning than nickel, however only copper (without CeO_2) with YSZ had a poor performance. Some other anode materials studied are Ni/ScSZ [6] and Ni/CGO [15–20]. Doped or undoped ceria oxides were studied since they have good performance, low material cost and are more resistant to sulfur tolerances. A very good review on different anode materials with respect to sulfur poisoning was published by Gong et al. [14].

There are fewer studies on the poisoning behavior of Ni/CGO anodes when compared to Ni/YSZ anodes. Trembly et al. [15] tested the Ni/CGO anode with syngas mix of 34.8% H_2/35.7% N_2/40% CO with 207–235 ppm H_2S at 850 °C. The power immediately dropped 6–8% after 207 ppm H_2S addition and then slowly stabilized with totally 10–12.5% degradation. In another experiment, within the H_2S removal, the power recovery was 97%. With FESEM and EDX analysis they found sulfur and decreased amount of nickel in the anode and observed morphological change. NiS formation was the proposed mechanism. Another study of the same group [16] tested the H_2S effect on short stack with syngas mix of H_2/N_2/CO/H_2O with 120 ppm H_2S. They observed immediate drop of stack power (~10%) with addition of H_2S and a continuous degradation afterwards. However, they mentioned that the stack power decreased continuously before H_2S addition, too. For this reason, the continuous degradation cannot be interpreted as H_2S effect only.

According to Lohsoontorn et al. [17] the performance of a Ni-CGO/YSZ/Ni-CGO symmetrical cell decreases when pH_2 (9.7%, 48.5%, 97% H_2) and temperature decreases (600 °C–557 °C) and when pH_2S (1–3 ppm) increases. With increasing pH_2 the recovery of the cell increased, too. Using electrochemical impedance spectroscopy, they found that the performance loss was a result of the increase of the resistance due to charge transfer. With high pH_2S and low pH_2, sulfur was found to affect both charge transfer and mass transport. With thermodynamical calculations they found that the Ni–H_2S interaction depends on pS_2 and temperature and ceria–H_2S interaction on pO_2 and pS_2. Their thermodynamical calculation bases on the CeO_x-pS_2 system, however, it is known that the doped ceria with oxygen ion vacancy is not an effective sulfur adsorbent as ceria oxide (CeO_2) [14]. The temperature region is also lower than high temperature SOFC operating temperature. For this reason, the calculation results may not be adequate for SOFCs operating at temperatures higher than 600 °C. According to Aravind [18] up to 9 ppm H_2S addition in H_2/H_2O fuel at 800–1000 °C had no significant effect on the impedance of button cell with Ni/CGO anode after 1.5 h operation.

The only study which directly compares the performance of Ni/YSZ and Ni/10CGO anodes with H_2S known to the authors is published by Zhang et al. [19]. They compared the button cell performances with 5–700 ppm H_2S in H_2 at 800 °C for 2 h. They found that the voltage of the button cells with Ni/YSZ anode and Ni/CGO anode decreased from 0.61 V to 0.34 V and from 0.78 V to 0.72 V, respectively. They explain the positive effect of CGO with its mixed ionic electronic conductivity. The SEM analysis after contamination with 700 ppm H_2S showed rougher Ni surface formation for both of the anodes whereas YSZ was not affected. The surface of the CGO was not smooth but smaller CGO particles were formed after the experiment. The authors explained this behavior with the formation of Ce_2O_2S. No sulfur was found in both of the anodes with EDX.

In this study, the effects of H_2S in fuel (1–50 ppm) on the performances of single cell stacks with Ni/YSZ and Ni/CGO anodes are directly compared under various parameters at 850 °C. The study aims to understand the differences of H_2S poisoning and

regeneration mechanisms for Ni/YSZ and Ni/CGO anodes by evaluating the experimental results and already existing literature on the anode reaction mechanisms.

2. Experimental

Two types of electrolyte supported planar fuel cells were examined for the study. The cells with Ni/8YSZ anodes had a 30–50 μm thick Ni/8YSZ anode, a 150–200 μm thick 3YSZ electrolyte and a 30–50 μm thick LSM/8YSZ cathode manufactured at Fraunhofer IKTS, Germany. The cells with Ni/10CGO anodes had a 30–50 μm thick Ni/10CGO anode, an 80–110 μm thick 3YSZ electrolyte and a 30–50 μm thick LSM/8YSZ cathode manufactured at HC Starck GmbH, Germany. The electrolytes were fabricated by tape casting and the anode and cathode layers were applied using screen printing techniques. The active areas were 4 cm × 4 cm.

Electrochemical tests were performed with stacks with chromium-iron alloy bipolar plates (70 mm × 70 mm × 6 mm) (manufactured by Plansee SE, Austria) sealed with BaO–Al_2O_3–SiO_2 glass sealings. The cathode side of the bipolar plates were covered with cobalt, manganese and iron spinel (applied by roll coating) to minimize chromium poisoning of the cathode. The anode side of the bipolar plates were covered with 10 μm thick nickel coating (applied by galvanization method) for improved electrical contact. Contacting elements (between the bipolar plates and the MEA) were nickel mesh and silver mesh for the anode and cathode, respectively. 0.17 mm and 1 mm thick platinum wires were connected to bipolar plates using spot welding for voltage monitoring and current drawing, respectively. Both the anode and cathode gases were supplied and exhausted from the base of the stack. The flow configuration in the stacks was cross-flow (Fig. 1).

The gases were supplied through mass flow controllers. H_2O was mixed with anode gas mixture with an evaporator. For H_2S contamination, a part of N_2 was replaced with a certified gas amount of 1000 ppm H_2S/N_2 mixture just before the fuel inlet of the stack in order to prevent H_2S dissolution in the evaporator and sulfur adsorption in the piping while the total fuel flow was kept constant at 40 L h^{-1}. As cathode gas 40 L h^{-1} dry air was used. The stacks were sealed as well as reduced at 930 °C. The reduction was performed by increasing the H_2 content in N_2 stepwise. At the end of the reduction the anode gas was consisted of 100% H_2. The stacks were then cooled down to 850 °C followed by the activation of the cell by applying a constant current load with operating fuel composition where cell voltage increases at about first 100 h. The stacks were then characterized electrochemically. The stacks were galvanostatically operated at 850 °C. If not otherwise stated the fuel composition was 43.8% H_2, 6.2% H_2O, 50% N_2. Low fuel utilization (16–24%) was chosen in order to reduce the concentration overpotentials and to expose the anode to possibly similar conditions at the fuel inlet and fuel outlet of the cell. This gives the possibility to investigate the effects of the gas composition. It should be noted that in real systems the fuel utilization values will be higher (60–80%) to achieve higher electrical efficiencies. High fuel utilization corresponds to high steam content in the fuel. Very high steam concentrations may have an effect on the mechanisms of H_2S poisoning. The impedance measurements were carried out in potentiostatic mode using sinusoidal signal amplitude of 10 mV over the frequency range of 50 kHz to 0.01 Hz using Zahner Zennium workstation.

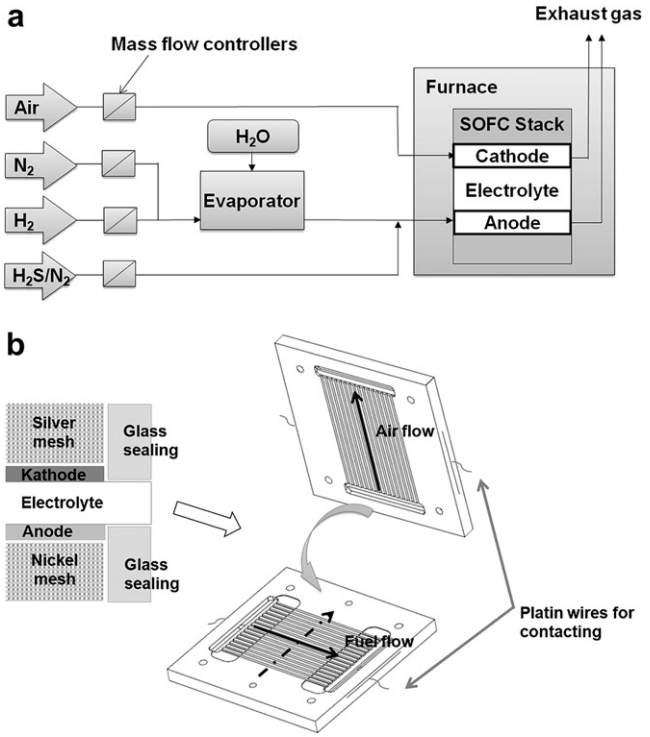

Fig. 1. Schematic illustration of a) the experimental setup, b) the stack assembly.

3. Results

In this chapter, the results of the experiments with different parameters are presented. The mechanisms will be discussed in the discussion chapter based on the obtained results in this section.

3.1. Single H_2S contamination

The stacks with Ni/8YSZ and Ni/10CGO anodes operated at 850 °C with 43.8% H_2, 6.2% H_2O and 50% N_2 were contaminated with 2 ppm H_2S for a period of 15 h. Stack current densities were kept constant at 319 mAcm^{-2} and at 225 mAcm^{-2} for the stacks with Ni/8YSZ and Ni/10CGO anodes with constant voltages of 0.74 V and 0.71 V with 24% and 18% fuel utilization, respectively. Fig. 2 displays the percental changes of the cell voltages as a function of time for both of the stacks with respect to sulfur poisoning.

The cell voltages responded differently to H_2S addition. First, there was an immediate voltage drop for both of the cells with 2 ppm H_2S addition to the fuel (Phase 1). With Ni/8YSZ anodes, the cell voltage degradation (dU/U_0) was 11.70% in the first 30 min of

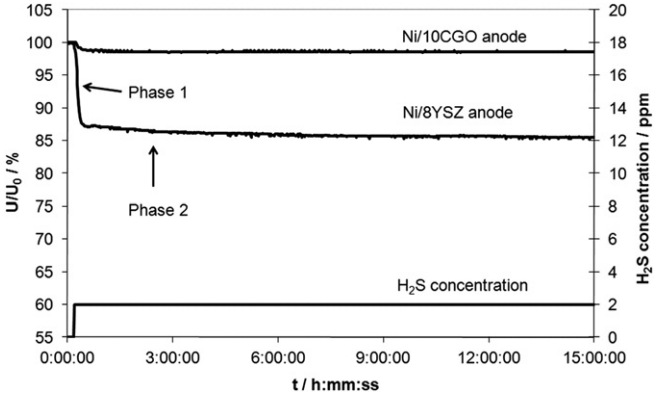

Fig. 2. Comparison of the ratios of the contaminated stack voltages to initial stack voltages with respect to time with Ni/8YSZ and Ni/10CGO anodes exposed to 2 ppm H_2S at 850 °C.

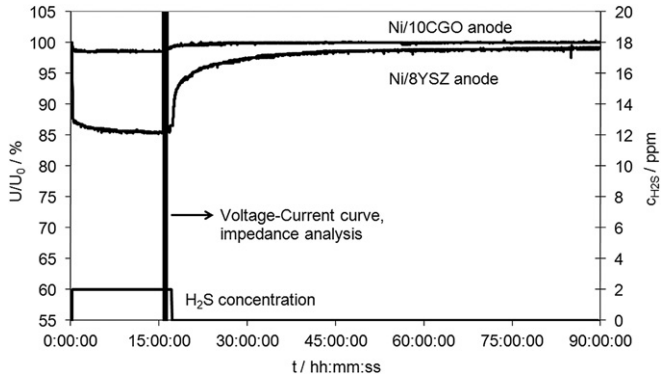

Fig. 3. Comparison of the ratios of the contaminated stack voltages to initial voltages with respect to time with Ni/8YSZ and Ni/10CGO anodes during and after 2 ppm H_2S contamination at 850 °C.

contamination. This voltage decrease was followed by a slow drop with total degradation rate of 13.51% over the next 12 h (Phase 2). Saturation status was then seemed to be achieved. With Ni/10CGO anode, the rapid cell voltage degradation (dU/U_0) was 1.3% in the first 30 min. The cell voltage was then constant (Fig. 2).

After 15 h of contamination H_2S was removed from the fuel. As removing H_2S, an immediate increase of the cell voltage for both of the stacks was observed. After 90 h of operation, the cell voltages reached constant values of 98.9% and 100% for the stacks with Ni/8YSZ and Ni/10CGO anodes, respectively (Fig. 3).

The recovery was slower than the poisoning for both of the stacks. The results showed that the 2 ppm H_2S poisoning of Ni/8YSZ stack was irreversible whereas Ni/10CGO stack poisoning was reversible.

3.2. Multiple H_2S contaminations

In further test series, multiple H_2S poisoning procedure was performed since in a functioning SOFC system, a stack can be subjected to H_2S poisoning for several times. For the experiment, contamination procedure explained in previous section was repeated four more times under same experimental conditions with the same stacks with regeneration phases in between. Fig. 4 displays the ratio of the contaminated (U_{H2S}) and regenerated (U_{reg}) cell voltages to the initial cell voltage (U_0) for each contamination cycle with 2 ppm H_2S at 850 °C. The stack with Ni/8YSZ anode lost almost 25% of its power after five contamination cycles whereas the voltage of the stack with Ni/10CGO anode was almost

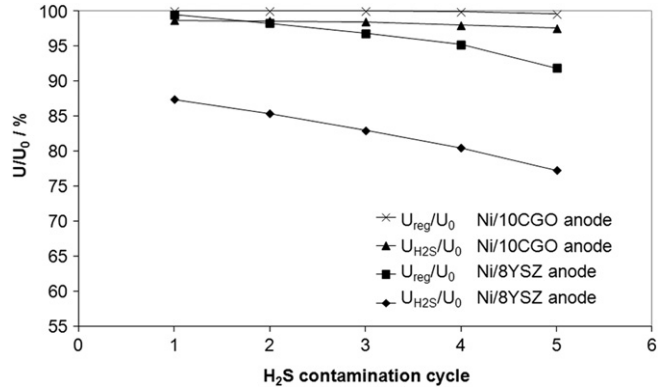

Fig. 4. The variation of stack voltage ratios to initial voltages with H_2S contamination/regeneration cycles.

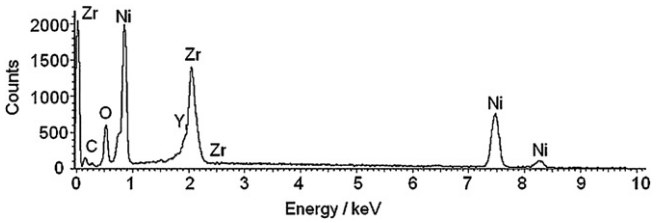

Fig. 5. Qualitative EDX analysis of the Ni/8YSZ anode after 2 ppm H_2S contamination/regeneration cycles at 850 °C.

constant. After 5 contamination cycles, the stack voltage decreased to 97.6% of the initial value for Ni/10CGO stack. After the last regeneration phase, the stack voltage reached to 99.7%. For the stack with Ni/8YSZ anode this value was just 91.8% (Fig. 4).

The Ni/8YSZ anode was analyzed with FESEM (Zeiss, LEO DSM 982) and EDX (INCAx-sight, Oxford Instruments) as the stack was cooled down to room temperature with forming gas (5% H_2, 95% N_2). H_2 containing gas without H_2S was used to cool the stack in order to prevent anode from nickel sulfide formation at low temperatures and nickel oxide formation through leakages in the stack inlets. Even though the stack with Ni/8YSZ anode lost approximately 10% of its' voltage no sulfur traces or changes in the microstructure were observed (Fig. 5).

Due to high detection limit of EDX to detect sulfur if there is any, it was decided to analyze the Ni/8YSZ anode (sample a) with TOF-SIMS (TOF-SIMS.5-100P, ION-TOF GmbH). Two other samples were also analyzed to compare the sulfur intensities: a reference MEA (sample b) operated with 50% H_2, 50% H_2O at 850 °C for 335 h and a MEA (sample c) operated with 43.8% H_2, 6.2% H_2O, 50% N_2 at 850 °C for 500 h, last 15 h with 50 ppm H_2S. No regeneration was followed. The samples were analyzed with the depth profiling method to determine the distribution of sulfur as a function of depth from the anode surface. An area of 300 × 300 μm^2 was bombarded with a primary ion dose density of $1.36.10^{17}$. The Ni, YSZ and S intensities of the samples are summarized in Table 1.

The lowest sulfur intensity was found in sample b which is expected since the anode was not exposed to sulfur. The sulfur intensity (90) there should be the accepted as an analysis error. The sample contaminated with the highest concentration of sulfur (50 ppm) showed the highest sulfur intensity among the investigated samples. Even though sample a had an 80 h of regeneration phase, it is shown that a sulfur amount is left in the anode. The sulfur traces found in the anode show that desorption of sulfur from the anode surface is not complete and may therefore still block the adsorption sites in the anode. The total power recovery of the stack performance was therefore not observed.

3.3. Effect of H_2S concentration

The H_2S concentration, particularly the pH_2S/pH_2 ratio, may have an influence on the poisoning rate of the stacks. Fig. 6 shows the U/U_0 ratio of the stacks with different H_2S concentrations in

Table 1
The average depth profile intensities of nickel, zirconium oxide and sulfur in the samples analyzed with TOF-SIMS.

Element/ molecule	Intensity		
	a	*b*	*c*
Ni	70000	70000	60000
ZrO_2	4000	4000	4000
S	500	90	1500

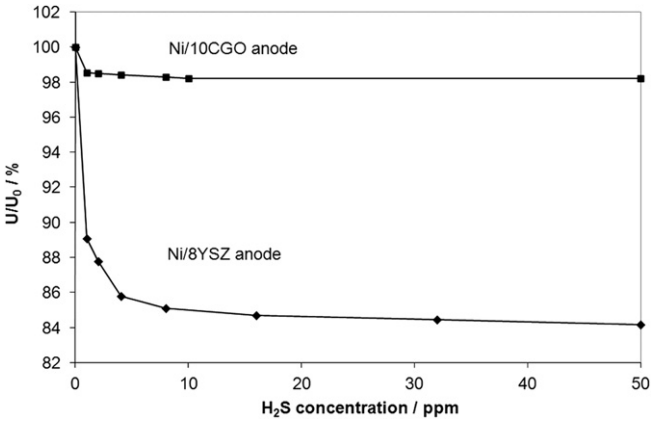

Fig. 6. Comparison of H_2S concentration dependence of the stack voltages with Ni/8YSZ and Ni/10CGO anodes.

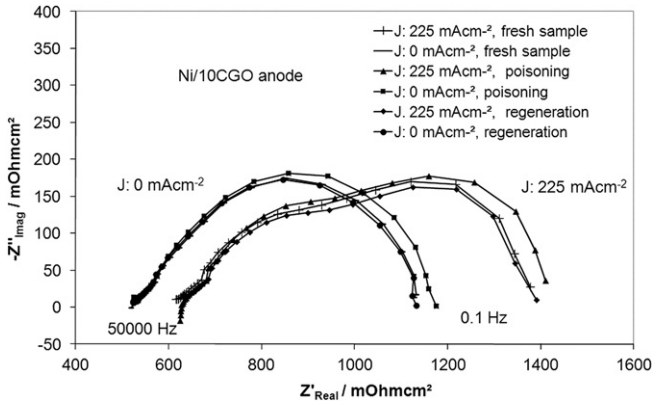

Fig. 8. Comparison of the impedance spectra of the Ni/10CGO stacks before, during and after 2 ppm H_2S poisoning operating with 225 $mAcm^{-2}$ and 0 $mAcm^{-2}$ current densities.

43.8% H_2, 6.2% H_2O, 50% N_2 fuel gas which run with 24% fuel utilization. For the experiments, H_2S in various concentrations were added for 30 min to the fuel one after other. The stacks were poisoned with 1–50 ppm H_2S. For both type of the stacks, the highest degradation rate was achieved with addition of 1 ppm H_2S to the H_2S free fuel. H_2S concentration increase had a very low effect on the degradation rate with Ni/10CGO anodes. The stacks with Ni/8YSZ anodes responded more to the increase of H_2S concentration.

3.4. Effect of applied current

The effect of applied current on the H_2S poisoning behavior of the stacks with Ni/8YSZ and Ni/10CGO anodes are demonstrated in Fig. 7 and Fig. 8, respectively. Four different single cell stacks were tested for this purpose. The impedance spectra of the stacks run with and without current at 850 °C with 43.8% H_2, 6.2% H_2O, 50% N_2 and 2 ppm H_2S were measured and compared between the frequency ranges 50,000 Hz–0.1 Hz and with 50 mA DC current for both type of the anodes. The fuel utilizations of the stacks operating with current were about 24%. Same procedures were applied to the stacks as in section 3.1. The impedances of the fresh (initial), poisoned and regenerated stacks are compared for both types of the stacks.

According to Fig. 7, the stacks with Ni/8YSZ anodes operated with and without current have the same impedance spectra before poisoning. As the stacks were poisoned with 2 ppm H_2S, the impedance of both stacks increased evidently whereas the stack run without current had more increase in the intermediate and low frequency range than the stack run with current. The increase of the impedances at low frequencies can be attributed to the increase of resistances in the anode due to hindered hydrogen adsorption on nickel surface coupled with charge transfer reactions connected with H_2S addition. With H_2S removal, the impedance of both of the stacks didn't reach to initial values whereas the stack run without current had higher impedance than the stack run under load. The ohmic resistances of the stacks remained same throughout the experiments. The results indicate that current flow has a positive effect on the sulfur resistance of the stacks.

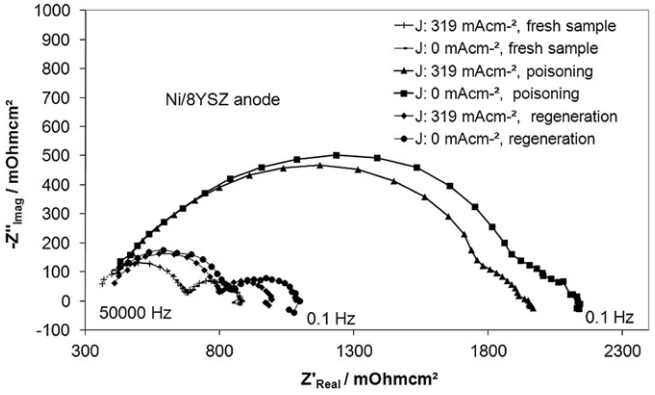

Fig. 7. Comparison of the impedance spectra of the Ni/8YSZ stacks before, during and after 2 ppm H_2S poisoning operating with 319 $mAcm^{-2}$ and 0 $mAcm^{-2}$ current densities.

Fig. 8 shows that, unlike with Ni/8YSZ anodes, current density has no effect on the impedance behavior of the Ni/10CGO anodes. The shift of the real part of the impedance between stacks run with and without current is the result of differences in resistance due to component tolerances scattering by stack manufacturing. The small increase of the impedance with addition of H_2S is similar for both stacks. With H_2S removal, the impedances reach to their initial values. The results indicate that current flow has no effect on the H_2S poisoning behavior of Ni/10CGO stacks.

3.5. Effect of H_2O concentration

The positive effect of current density on H_2S resistance of Ni/8YSZ anodes reveals the question whether this effect depends on the partial pressure of water. Therefore, the effect of H_2O concentration was studied with two fuel types containing different concentrations of water with 2 ppm H_2S addition. Hydrogen concentrations were kept constant in order to have equal pH_2S/pH_2 values. The compositions were balanced with nitrogen (Table 2). The fuel compositions for the stacks were set as "Inlet" concentrations as shown in Table 2. The fuel utilization was 16%. The outlet water concentrations differ from inlet concentrations due to the applied current density of 200 $mAcm^{-2}$ and are calculated using Faraday's law.

Table 2
Inlet and outlet fuel compositions. (J: 200 $mAcm^{-2}$, F_U: 15.2%).

		pH_2O/pH_2	H_2/Vol %	log pH_2	H_2O/Vol %	log pH_2O	N_2/Vol %	log pN_2
Fuel 1	Inlet	0.14	43.8	−0.36	6.2	−1.2	50	−0.3
	Outlet	0.35	37.1	−0.43	12.9	−0.89	50	−0.3
Fuel 2	Inlet	0.57	43.8	−0.36	24.8	−0.6	31.4	−0.5
	Outlet	0.85	37.1	−0.43	31.5	−0.5	31.4	−0.5

The impedance spectra were recorded before H_2S poisoning and after 24 h of regeneration for both of the stacks. The Nyquist plots are shown in Fig. 9. According to the diagram, the ohmic resistances have similar values ($\sim$700 mOhmcm^{-2}) whereas for higher water concentrations the impedance is lower. This is due to lower conversion impedance with higher H_2O content. It was also reported that water vapor enhances the oxygen surface exchange rate both on the metal and YSZ surfaces of Ni/YSZ anodes [20,21] and therefore affect the electrode polarization and consequently also to the impedance in a positive way since conversion of the fuel gas itself in the electrode reaction contribute to the electrode polarization. However, the addition of H_2S to fuel causes similar increase of the impedance of the regenerated stacks for both fuel types which shows that pH_2O in fuel has no influence on H_2S poisoning/regeneration.

4. Discussion

In presence of sulfur in the anode sulfur adsorption and sulfide formation are two possible mechanisms. Thermodynamical calculations show that the formation of nickel sulfide with several ppm of H_2S at high temperatures is not favorable [6]. The adsorption process takes place at H_2S/H_2 ratios far lower than the ratios for sulfide formation [22]. Our thermodynamical calculations also confirm this result (Fig. 10).

Additionally, no morphological changes of the anode, which show any sulfide formation, were observed with FESEM and EDX analyses. For this reason, the voltage degradations in this study cannot be explained by sulfide formation.

Studies on the kinetics of H_2S adsorption on metals state that the adsorption of H_2S on metals is quite rapid and the high sticking probability suggests that no barrier to adsorption and dissociation exists until saturation is approached [23]. Stable saturation uptakes of sulfur were observed at $H_2S/H_2 = 1–10 \times 10^{-6}$ up to $100–1000 \times 10^{-6}$ above which formation of bulk sulfide takes place which means that the saturation layer is stable at H_2S/H_2 ratios several magnitudes below the ratios for sulfide formation [24]. Based on the density functional theory calculations the dissociative adsorption was found to be the dominant reaction [25]:

$$Ni_{(s)} + H_2S_{(g)} \rightarrow Ni_{(s)} - SH_{(s)}{}^{*} + H_{(s)} \rightarrow Ni - S_{(s)} + 2H_{(s)} \qquad (1)$$

where s, g, and asterisk stand for surface, gas, and a different adsorbed intermediate.

The adsorption isotherms at various temperatures under H_2 and H_2S gas mixtures were experimentally studied to determine the energy of adsorption by some groups. McCarthy and Wise [26] and

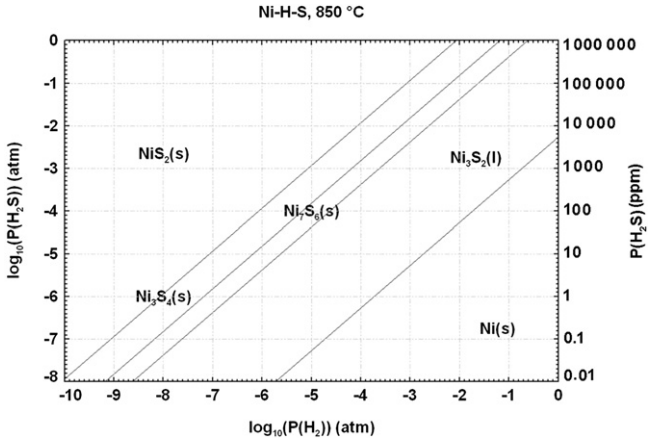

Fig. 10. Thermodynamical calculation of $\log_{10}(P(H_2))$ versus $\log_{10}(P(H_2S))$ for the nickel-sulfide system at 850 °C with FactSage®. The lowest H_2S concentration for nickel sulfide formation with 50 vol% H_2 in the fuel gas is approximately 2500 ppm H_2S.

Oliphant et al. [27] have determined the heat of adsorption for Ni/Al_2O_3 in a range of (ΔH_{ad}: -150 kJ mol^{-1}) that decreases slowly at high temperatures which is energetically more favorable than the heat of formation of bulk sulfide (ΔH_f: -75 kJ mol^{-1}) on various forms of nickel. Attempts to correlate the data with Langmuir-Type isotherm were not successful because of departures from the Langmuir model due to the strong interaction between adsorbed atoms, high surface mobility and the dependency on the surface coverage [24]. Rostrup-Nielsen proposed the following Temkin like isotherm [24] to correlate data:

$$\frac{p_{H_2S}}{p_{H_2}} = \exp\left(\Delta H^0 \cdot (1 - (\alpha \cdot \theta))/R \cdot T - \Delta S^0/R\right) \qquad (2)$$

where α is constant and θ is the fractional coverage of nickel surface. The results were well described with $\Delta H^0 = 289$ kJ mol^{-1}, $\Delta S^0 = -19$ kJ mol^{-1}K^{-1} and $\alpha = 0.69$ [24] which formed the equation:

$$\theta = 1.45 - 9.53.10^{-5} \cdot T + 4.17.10^{-5} \cdot T \cdot \ln\frac{p_{H_2S}}{p_{H_2}} \qquad (3)$$

As in Temkin theory, this model predicts a linear increase in the enthalpy with increase of the coverage but entropy is independent from coverage. It was shown with this equation that even with very low H_2S concentrations the coverage of the nickel surface with sulfur will be high.

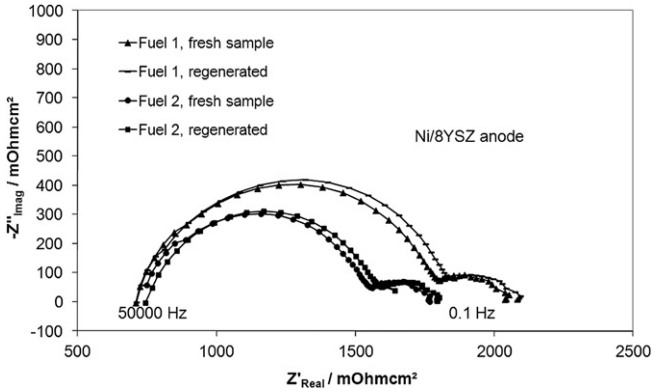

Fig. 9. Comparison of Nyquist plots of the stacks before poisoning and after 24 h of regeneration.

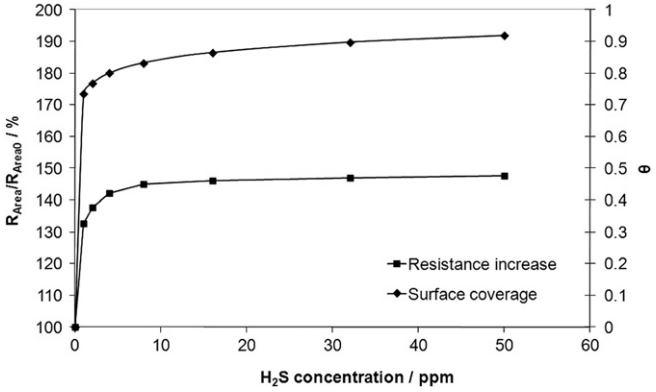

Fig. 11. Effect of H_2S concentration on cell resistance increase with Ni/8YSZ anode and calculated surface coverage using Eq. (3).

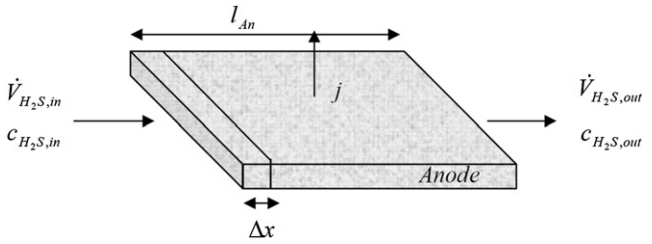

Fig. 12. Progress of sulfur contamination of the anode beginning from the fuel inlet to the fuel outlet.

Since the adsorption of sulfur on oxides is negligible at low H_2S concentrations [23] this value represents a good approach for the sulfur adsorption on Ni/YSZ and Ni/CGO cermets. It was shown that CeO_2 does not react with H_2S when H_2S concentration is below 450 ppm at 800 °C. At higher concentrations Ce_2O_2S may form [13]. On the other hand doped ceria with oxygen ion vacancy is not an effective sulfur adsorbent as ceria oxide [28].

In 3.3, the effect of the H_2S concentration on stack voltage degradation was studied. It was shown that the cell voltage decreases even with low H_2S concentrations (1 ppm) in fuel but the saturation was almost stable with 10 ppm H_2S. The calculated nickel surface coverage values for the experimental parameters with Eq. (3) correlates well with the observed increase of the cell resistances with Ni/8YSZ anode in our study (Fig. 11).

In an SOFC stack, if the adsorption of H_2S on nickel surface is quite rapid, it should first contact the nearest anode surface (fuel inlet) and rapidly adsorb on the nickel surface as soon as H_2S is added to fuel. Simplified schematic of an anode surface with the contaminated length is presented in Fig. 12. The thickness of the anode in this simplified model is not taken into consideration.

The contaminated length is given as Δx in the figure. The relationship of whole area specific resistance to the contaminated and uncontaminated area specific resistances (R_{Area}) is dependent on the length of contaminated area and can be expressed in terms of cell potential as follows:

$$R_{Area} = \frac{A_{An}}{I}\cdot\frac{1}{l_{An}}\cdot\int_0^l (U_0 - U(x))dx \tag{4}$$

If we assume that Δx is known, it is possible to calculate the area specific resistance:

$$\frac{1}{R_{Area}} = \frac{1}{R_{Area,0}\cdot\dfrac{l_{An}}{l_{An}-\Delta x}} + \frac{1}{R_{Area,con}\cdot\dfrac{l_{An}}{\Delta x}} \tag{5}$$

where $R_{Area,0}$ is the area specific resistance of uncontaminated and $R_{Area,con}$ is the contaminated area. If we consider that there is a direct relationship between contaminated length (Δx) and duration of total voltage decrease during phase 1 (t_{PhI}) and duration of voltage decrease (Δt), the relation can be written as:

$$\Delta x = \frac{l_{An}}{t_{PhI}}\Delta t \tag{6}$$

R_{Area} is then:

$$R_{Area} = \frac{R_{Area0} + R_{Areacon}}{R_{Areacon}\cdot\left(1-\dfrac{\Delta t}{t_{PhI}}\right) + R_{Area0}\cdot\dfrac{\Delta t}{t_{PhI}}} \tag{7}$$

As an example a stack with Ni/8YSZ anode is contaminated with 1 ppm H_2S. The resistance of the stack is calculated with the equation above and compared with the real resistance increase during phase 1 (Fig. 13).

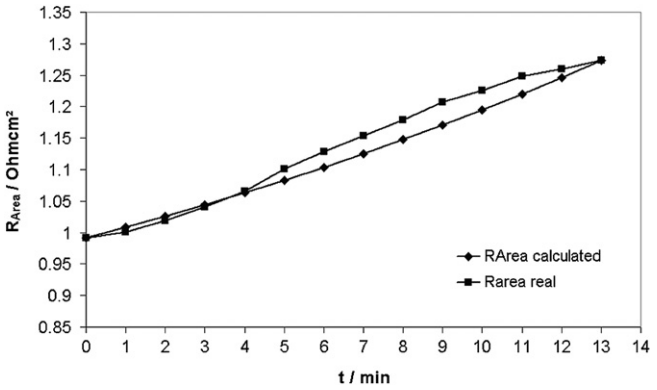

Fig. 13. Comparison of the calculated and real (observed) area specific resistances.

The calculated R_{Area} has an almost linear behavior whereas the real R_{Area} increase begins with a delay and flattens at the end of the phase 1. The delay of the resistance increase can be explained by considering the time required to flash the anode compartment with H_2S. As the concentration reaches 1 ppm at the inlet of the anode, R_{Area} increases linearly with time. The flattening effect at the end is caused by the decreasing rate of sulfur adsorption; due to the decreasing probability of each sulfur atom finding a vacant adsorption site on the nickel surface (with increasing coverage of the nickel surface with sulfur).

If it is assumed that H_2S that hits the anode surface is homogeneously distributed and every sulfur atom that hits the surface adsorbs on nickel, one can calculate the nickel surface area accessible for sulfur adsorption (A_{Ni}) as:

$$A_{Ni} = \frac{\dot{n}_{H_2S}\cdot t_{PhI}}{c_{sat}} \tag{8}$$

where c_{sat} is sulfur saturation concentration observed as $8.37.10^{14}$ sulfur atoms per 1 cm^2 polycrystalline nickel surface ($1.39.10^{-9}$ mol sulfur per cm^2 nickel) by Oudar [29]. An experiment was performed to confirm the relationship between H_2S concentration and t_{PhI}. A stack with a Ni/8YSZ anode was contaminated with 1 ppm, 2 ppm, 4 ppm and 8 ppm H_2S. The fuel composition was 43.8% H_2, 6.2% H_2O, 50% N_2 with 24% fuel utilization. Fig. 14 shows the data recorded between 30 min before and 60 min after H_2S addition. t_{lin} for 1 ppm, 2 ppm, 4 ppm and 8 ppm H_2S contamination were recorded as 13 min, 6 min, 3 min and 1.5 min, respectively, which is in consistence with Eq. (8).

In Fig. 15 the linear relation between $1/t_{PhI}$ and H_2S concentration is shown. The linear relationship confirms the proposed progress of anode poisoning with sulfur.

If it is considered that adsorption on the nickel surface takes place only during phase 1, the poisoned nickel surface area can be calculated with Eq. (8). With 40 ± 0.2 L h^{-1} total fuel volume flow under ideal gas conditions, the H_2S molar volume flow rates can be calculated. The approximate poisoned nickel surface area (A_{Ni}) calculated with Eq. (8) is found to be 0.027 m^2. This is an approximate value due to the nonlinear behavior of voltage decrease at the beginning and end of phase 1 which makes t_{Ph1} inaccurate.

The sulfur adsorption mechanism on nickel surface will be the same for the Ni/8YSZ and Ni/10CGO anodes however Ni/10CGO anodes showed much better resistance to sulfur poisoning.

CGO has a superior feature of being a mixed ionic electronic conductor at low pO_2 when compared to YSZ. Ceramics based on CeO_2 show activity for electrochemical oxidation in SOFCs in

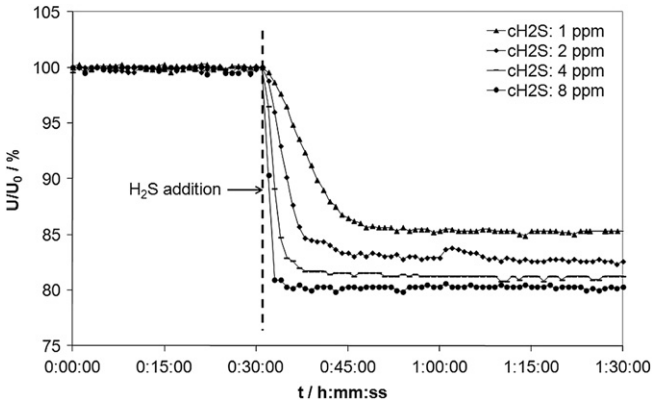

Fig. 14. Voltage drop as a function of H_2S concentration and time.

reducing environments at $T>500$ °C due to the reduction of Ce^{4+} to Ce^{3+} [30,31]. The ability of CGO to transport electrons as well as oxygen ions extends the triple phase boundaries to a large extent. Primdahl et al. [32] compared the oxygen and electronic conductivities of 8YSZ and 10CGO at 850 °C with 97% H_2/3% H_2O fuel. The oxygen ionic conductivities are 0.07 Scm^{-1} and 0.06 Scm^{-1} for 8YSZ and 10CGO, respectively. The electronic conductivity of 10CGO however is 2 Scm^{-1} whereas 8YSZ has only 1×10^{-5} Scm^{-1}. Additionally the ability of CGO to adsorb hydrogen extends the triple phase boundaries within Ni/CGO anode [33,34].

In Ni/YSZ anodes, the dissociative adsorption of H_2 and H_2O takes place on the nickel surface in the absence of H_2S in the gas phase. It is assumed that the adsorption of hydrogen on the YSZ surface is very small and therefore can be neglected [35]. YSZ surface will be active for the chemisorption of water and the formation of hydroxyl [36]. However due to the complexity, it is not included. It should also be noted that water indirectly helps to enhance the surface exchange rate of oxygen on the surface of YSZ [20]. The charge transfer reaction is assumed to take place in one step on the Ni-YSZ interface [36]. When H_2S is added to the fuel, H_2S immediately dissociatively adsorbs on the nickel surface. Since H_2S adsorption is more favorable [23], hydrogen adsorption on nickel as well as the charge transfer reaction is hindered. With oxygen ion flux, the adsorbed sulfur on TPB will react with O^{2-} to form intermediate SO_2, however SO_2 will be a transient molecule since it will immediately react with H_2 to form H_2S under given conditions (Fig. 16).

In case of Ni/CGO anodes, the reactions on the nickel surface are similar to those with Ni/YSZ anodes. When H_2S is added to the fuel, H_2S immediately dissociatively adsorbs on the nickel surface. However, hydrogen solubility in the doped ceria allows the hydrogen adsorption reactions to take also on CGO surface. The high electronic conductivity of CGO allows transferring the released electrons. With oxygen ion flux, similar to reactions with YSZ, the adsorbed sulfur on TPB will react with O^{2-} to form intermediate SO_2. However, H_2 and H_2O adsorption and electronic conductivity can take place also on CGO. This explains the low voltage drop by sulfur addition to the fuel which blocks only nickel surfaces and has no effect on CGO due to its oxidic nature. The TOF-SIMS analyses of Ni/8YSZ anodes also showed that sulfur doesn't desorb completely from nickel surface even with regeneration which explains the incomplete performance coverage of the stacks with Ni/8YSZ anodes. The incomplete desorption doesn't effect the reactions in CGO and therefore the performance of the Ni/CGO anodes. Due to these reasons, Ni/CGO anodes have more resistivity towards sulfur poisoning when compared to Ni/YSZ anodes. The proposed electrochemical processes in the Ni/8YSZ and Ni/10CGO anodes with and without H_2S in H_2/H_2O fuel are shown in Fig. 16.

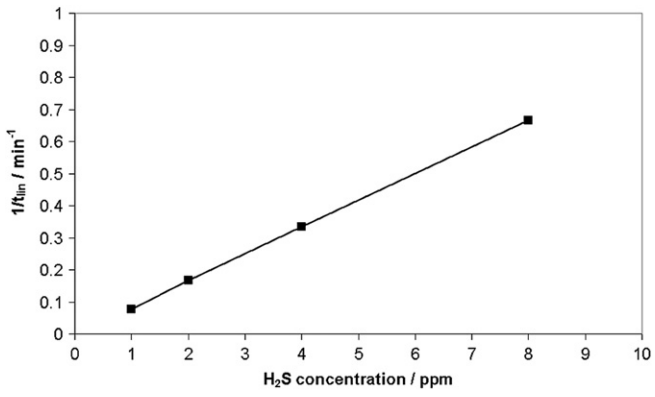

Fig. 15. Linear relation between $1/t_{lin}$ and H_2S concentration.

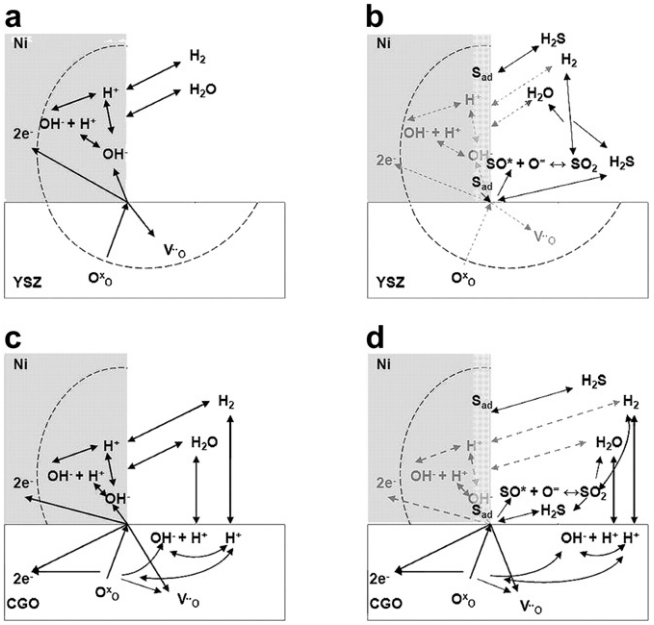

Fig. 16. Proposed electrochemical processes in the anode around H_2–H_2O/Ni/YSZ interface a) without H_2S, b) with H_2S. Proposed electrochemical processes for H_2 oxidation around H_2–H_2O/Ni/CGO interface c) without H_2S and d) with H_2S. The thicknesses of the arrows in the figure are not relevant.

5. Conclusions

In this work, the performances of stacks with Ni/8YSZ and Ni/10CGO anodes with respect to sulfur poisoning in $H_2/H_2O/N_2$ fuel have been compared. The stacks with Ni/10CGO anode showed much better resistivity to sulfur than the stacks with Ni/8YSZ anodes. The addition of 2 ppm H_2S to the fuel decreased the single cell stack voltages with Ni/8YSZ and Ni/10CGO anodes to 86.5% and 98.7% of their initial voltages, respectively. The stack with Ni/8YSZ anode had two poisoning stages whereas with Ni/10CGO had a one stage poisoning. At the first stage the voltages decreased quickly in few minutes. This phase was followed by a slower degradation in the following ~10 h for the stack with Ni/8YSZ anode. At the 15th hour the stack voltage was stable. During multiple sulfur poisoning cycles (5×2 ppm H_2S with regeneration phases in between) the stack voltage with Ni/8YSZ anode decreased with every H_2S

addition to lower values, caused at the end almost 25% voltage decrease. After 80 h regeneration phase the stack voltage recovered 91.8% of its initial value which shows that the more often the Ni/8YSZ anode is subjected to sulfur the higher will be the degradation rate. This effect was not observed for the stack with Ni/10CGO anode. No structural changes or sulfur were observed with FESEM and EDX analyses after the experiments. The TOF-SIMS analysis of Ni/8YSZ showed however sulfur traces in the anode which is the reason for the incomplete voltage regeneration. Even 1 ppm H_2S addition to H_2S free fuel caused high degradation rates (11% and 1.5% for Ni/8YSZ and Ni/10CGO anode, respectively) whereas the following concentration increase up to 50 ppm H_2S had less effect on the degradation rates which is in good consistence with the surface sulfur coverage values of nickel surface proposed by Rostrup-Nielsen [24]. A mechanism for the progress of the sulfur poisoning in the anode is proposed. It is shown that theoretically it is possible to calculate the nickel surface area poisoned by sulfur in the anode using H_2S poisoning behavior for Ni/8YSZ anodes. Sulfur poisoning mechanisms for both types of the anodes are proposed by taking account the proposed oxidation mechanisms of H_2 in the anodes by previous studies [20,23,32–36]. The higher sulfur resistance of Ni/10CGO is explained with its high mixed ionic electronic conductivity as well as its ability to adsorb H_2. Due to these properties CGO can continue electrochemical reactions when nickel is covered with sulfur. For this reason, surface coverage of nickel with sulfur has no effect on the performance of stacks with Ni/10CGO anodes. The long term poisoning effects and the effects of other fuels (CO, C_xH_y) should still be studied in detail in order to understand their effects on poisoning mechanisms.

Acknowledgment

The study is financed by Fraunhofer IKTS as a part of a PhD study. The authors gratefully acknowledge Staxera GmbH and H.C. Starck GmbH for their financial and material contributions.

References

[1] Technische Regel, Arbeitsblatt G 260, Gasbeschaffenheit, DVGW Regelwerk, 2008.
[2] Verordnung über die Beschaffenheit und die Auszeichnung der Qualitäten von Kraftstoffen – 10.BlmSchV (2004).
[3] Technische Regel, Arbeitsblatt G 262, Nutzung von Gasen aus regenerativen Quellen in der öffentlichen Gasversorgung, DVGW Regelwerk, 2004.
[4] S.K. Gangwal, Desulfurization for fuel cells, in: D. Shekhawat, J.J. Spivey, D.A. Berry (Eds.), Fuel Cells: Technologies for Fuel Processing, Elsevier, 2011, pp. 317–360.
[5] Y. Matsuzaki, I. Yasuda, Solid State Ionics 132 (2000) 261–269.
[6] K. Sasaki, K. Susuki, A. Iyoshi, M. Uchimura, N. Imamura, H. Kusaba, Y. Teraoka, H. Fuchino, K. Tsujimoto, Y. Uchida, N. Jingo, J. Electrochem. Soc. 153 (2006) A2023–A2029.
[7] S.C. Singhal, R.J. Ruka, J.E. Bauerle, C.J. Sprengler, in: US Department of Energy Report No. DOE/MC/22046-237 I, Washington D.C., 1986.
[8] J.H. Wang, M.L. Liu, Electrochem. Commun. 9 (2007) 2212–2217.
[9] J.W. Yun, S.P. Yoon, S. Park, H.S. Kim, S.W. Nam, Int. J. Hydrog. Energy 36 (2011) 787–796.
[10] S.H. Choi, J. Wang, Z. Cheng, M. Liu, J. Electrochem. Soc. 155 (2008) B449–B454.
[11] C.C. Xu, J.W. Zondlo, M.Y. Gong, F. Elizade-Blancas, X.B. Liu, I.B. Celik, J. Power Sources 195 (2010) 4583–4592.
[12] H. Kim, J.M. Vohs, R.J. Gorte, Chem. Commun. (2001) 2334–2335.
[13] H.P. He, R.J. Gorte, J.M. Vohs, Electrochem. Solid State Lett. 8 (2005) A279–A280.
[14] M.Y. Gong, X.B. Liu, J. Trembly, C. Johnson, J. Power Sources 168 (2007) 289–298.
[15] J.P. Trembly, A.I. Marquez, T.R. Ohrn, D.J. Bayless, J. Power Sources 158 (2006) 263–273.
[16] A.I. Marquez, T.R. Ohrn, J.P. Trembly, D.C. Ingram, D.J. Bayless, J. Power Sources 164 (2007) 659–667.
[17] P. Lohsoontorn, D.J.L. Brett, N.P. Brandon, J. Power Sources 183 (2008) 232–239.
[18] P.V. Aravind, J.P. Ouweltjes, E. de Heer, N. Woudstra, G. Rietveld, in: Proc. 9th International Symp, vol. 2005-07, Solid Oxide Fuel Cells, Electrochemical Society, NJ, USA, 2005, p. 1459.
[19] L. Zhang, S.P. Jiang, H.Q. He, X. Chen, J. Ma, X.C. Song, Int. J. Hydrog. Energy 35 (2010) 12359–12368.
[20] N. Sakai, K. Yamaji, T. Horita, Y.P. Xiong, H. Kishimoto, H. Yokokawa, J. Electrochem. Soc. 150 (2003) A689–A694.
[21] N. Sakai, K. Yamaji, T. Horita, H. Kishimoto, M.E. Brito, H. Yokokawa, Y. Uchimoto, Appl. Surf. Sci. 252 (2006) 7045–7047.
[22] J.R. Rostrup-Nielsen, J. Catal. 11 (1968) 220–227.
[23] C.H. Bartholomew, P.K. Agrawal, J.R. Katzer, Adv. in Catal. 31 (1982) 135–242.
[24] J.R. Rostrup-Nielsen. NATO Advanced Study Institute, Ser. E: Applied Sciences (1981) 209–227.
[25] Y.M. Choi, C. Compson, M.C. Lin, M.L. Liu, Chem. Phys. Lett. 421 (2006) 179–183.
[26] J.G. McCarty, H. Wise, J. Chem. Phys. 72 (1980) 6332–6337.
[27] J.L. Oliphant, R.W. Fowler, R.B. Pannell, C.H. Bartholomew, J. Catal. 51 (1978) 229–242.
[28] A. Tomita, K. Tsunekawa, T. Hibino, S. Teranishi, Y. Tachi, M. Sano, Solid State Ionics 177 (2006) 2951–2956.
[29] J. Oudar, Catal. Rev.-Sci. Eng. 22 (1980) 171–195.
[30] C.W. Sun, U. Stimming, J. Power Sources 171 (2007) 247–260.
[31] S.C. DeCaluwe, Ph.D. Thesis, University of Maryland, Maryland, 2009.
[32] S. Primdahl, M. Mogensen, Solid State Ionics 152 (2002) 597–608.
[33] N. Sakai, K. Yamaji, T. Horita, H. Yokokawa, Y. Hirahita, S. Sameshima, Y. Nigara, J. Mizusaki, Solid State Ionics 125 (1999) 325–331.
[34] S. Primdahl, Y.L. Liu, J. Electrochem. Soc. 149 (2002) A1466–A1472.
[35] C. Wagner, Ber. Bunsenges. Phys. Chem. 72 (1968) 778–781.
[36] A. Bieberle, Ph.D. Thesis, Swiss Federal Institute of Technology, Zürich, 2000.